Identification of three loci affecting HDL-cholesterol levels in a screen for chemically induced recessive mutations in mice[S]

Todd Juan,[†] Murielle M. Véniant,[*] Joan Helmering,[*] Philip Babij,[*] Daniel M. Baker,[§] Michael A. Damore,[§] Michael B. Bass,[**] Tibor Gyuris,[†] Mark Chhoa,[†] Chi-Ming Li,[†] Chris Ebeling,[††] Julie Amato,[††] George A. Carlson,[††] and David J. Lloyd[1,*]

Departments of Metabolic Disorders,[*] Protein Sciences,[†] Molecular Sciences,[§] and Computational Biology,[**] Amgen, Inc., One Amgen Centre Drive, Thousand Oaks, CA 91320; and McLaughlin Research Institute,[††] 1520 23rd Street South, Great Falls, MT 59405

Abstract **We conducted a genome-wide screen using the mutagen *N*-ethyl-*N*-nitrosourea to identify recessive mutations in genes that lead to altered lipid traits in mice. We screened 7,546 G3 mice that were of mixed C57BL/6J (B6)×C3.SW-*H2*^{b}/SnJ (C3) genomes and identified three pedigrees with differences in plasma HDL-cholesterol. Genome scan analyses mapped three distinct loci to chromosomes 3, 4, and 7. An S1748L missense mutation was identified in ABCA1 in one pedigree with undetectable levels of HDL-cholesterol and resulted in reduced protein levels. This phenotype was completely penetrant, semidominant, and cosegregated with high plasma triglycerides. Mice in a second pedigree had very high levels of plasma total cholesterol and HDL-cholesterol (up to 800 mg/dl total cholesterol). Despite a high degree of phenotype lability and reduced penetrance, an I68N missense mutation was identified in the transcription factor CCAAT/enhancer binding protein α (C/EBPα). Finally, a second high HDL-cholesterol pedigree of mice, again with a highly labile phenotype and reduced penetrance, was mapped to a 7 Mb locus on chromosome 3.** **These results illustrate the use of a hybrid background for simultaneous screening and mapping of mutagenized pedigrees of mice and identification of three novel alleles of HDL-cholesterol phenotypes.**—Juan, T., M. M. Véniant, J. Helmering, P. Babij, D. M. Baker, M. A. Damore, M. B. Bass, T. Gyuris, M. Chhoa, C-M. Li, C. Ebeling, J. Amato, G. A. Carlson, and D. J. Lloyd. **Identification of three loci affecting HDL-cholesterol levels in a screen for chemically induced recessive mutations in mice.** ***J. Lipid Res.*** **2009.** 50: **534–545.**

Supplementary key words hypercholesterolemia • mutagenesis • ATP binding cassette transporter A1

Cardiovascular disease (CVD) is the leading cause of death worldwide, and preventing atherosclerosis holds the key to reducing the burden of CVD (1). Atherosclerosis underpins the pathological basis for CVD, and is an inflammatory disorder that may be initiated by several factors. One of the most important factors is the elevation of LDLs in the circulation that enter the arterial wall to form a plaque. The buildup of plaque can eventually occlude the lumen and can prevent blood flow, ultimately leading to a heart attack. HDL is a protective risk factor for atherosclerosis (2). HDL is required to remove cholesterol from tissues and to effectively transport it to the liver (1). There, cholesterol is either secreted into bile or used for bile acid synthesis. This process is known as reverse cholesterol transport and is thought to be the predominant mechanism by which HDL modulates atherosclerotic plaque (3). The observations of *1*) an inverse correlation of high HDL levels and decreased cardiovascular events (4) and *2*) the regression of atherosclerotic lesions in rabbits infused with HDL (5) have prompted the search for therapies that elevate HDL for the prevention of CVD (6).

Genetics has played a significant role in the identification of genes that are involved in HDL biology. For example, Tangier disease (severe HDL deficiency) was found to be caused by a mutation in ABCA1 (7). Additionally, many other HDL genes have been found to be mutated in human monogenic disorders, including apolipoprotein A-I (apoA-I) (8), cholesteryl ester transfer protein (CETP) (9), hepatic lipase (LIPC) (10), lipoprotein lipase (LPL) (11), and lecithin:cholesterol acyltransferase (LCAT) (12). Mouse reverse genetics has also been lucrative with respect to understanding HDL function despite marked differences in human and rodent lipoprotein physiology (HDL being the most abundant lipoprotein species in mice) (13). Indeed,

Manuscript received 3 September 2008 and in revised form 15 October 2008.
Published, JLR Papers in Press, October 30, 2008.
DOI 10.1194/jlr.M800471-JLR200

[1] To whom correspondence should be addressed.
e-mail: dlloyd@amgen.com

[S] The online version of this article (available at http://www.jlr.org) contains supplementary data in the form of two tables.

the class B, type I, scavenger receptor (SR-BI) is a hepatic receptor essential for efficient HDL catabolism, and this role was revealed by analyzing mice engineered to harbor a defective SR-BI protein (14). The genetics of common HDL variation has recently been investigated in human populations using genome-wide association (GWA) analyses (15, 16). These studies have confirmed ABCA1, apoA-I, CETP, LIPC, LIPG, LPL, and LCAT as contributors to HDL variation in the general population (17). Similar studies have been conducted in mice as quantitative trait loci (QTL) analyses and have resulted in the identification of loci concordant with those found in human studies, demonstrating that the mouse is a reliable model for discovering new HDL genes for translation to human lipoprotein physiology (13, 18).

Few novel HDL genes have been uncovered from forward genetic studies of spontaneous mouse mutants (19, 20). Mutagenesis using the chemical mutagen *N*-ethyl-*N*-nitrosourea (ENU) is an efficient alternative method to provide the basis of an unbiased forward genetic screen in mice (21). The mutation rate using ENU is up to 3,000 times greater than the spontaneous mutation rate, and has led to the identification of a multitude of novel mouse alleles (www.informatics.jax.org) and many mutated genes (22).

Here we describe the results of this screen for recessive mutations and the mapping of three loci that produce distinct HDL-cholesterol phenotypes; the underlying mutations were identified for two of these three loci.

MATERIALS AND METHODS

Mouse breeding and mutagenesis

All mice were bred at McLaughlin Research Institute, which is accredited by the Association for Assessment and Accreditation of Laboratory Animal Care International. All procedures were reviewed and approved by the Institutional Animal Care and Use Committee.

To ensure accurate dosing and reproducible mutation rates, the concentration of ENU (Sigma-Aldrich, St. Louis, MO) was determined spectrophotometrically (23). B6 male mice were injected intraperitoneally three times with 100 mg ENU/kg body weight with 1 week between the injections. Fertility testing commenced 6 weeks after the last injection; fewer than 10% of the mice had a sterile period shorter than 8 weeks, and these mice were discarded. The average return to fertility was approximately 15 weeks after the last ENU injection. B6 mice have the disadvantage of being highly susceptible to thymic lymphoma following mutagen treatment, leading to attrition both before and after regaining fertility. Approximately 40% of the ENU-treated mice did not sire pups. Fertile ENU-treated B6 males were mated with C3 females to produce first-generation (G1) C3.B6F1 male pedigree founders. Each G1 male was mated with two to four C3 females to produce six to eight G2 daughters that were backcrossed to their G1 parent with the goal of producing at least 24 G3 mice from each pedigree for screening as rapidly as possible.

This outcrossing strategy was developed in a previous study, where its effectiveness was compared with that of a screen for recessive mutations in inbred B6 mice (M. Appleby, J. Amato, M. Brunkow, C. Ebeling, F. Ramsdell, K. Staehling-Hampton, R. Schatzman, and G. Carlson, unpublished observations). In the inbred screen, approximately 10% of heritable immunological phenotypes were successfully mapped. In B6 mice, approximately 70% of the phenotypes that were heritable were lost when outcrossed for mapping. The average interval between identification of a phenodeviant in inbred B6 mice and determining a chromosomal location was approximately 8 months. In contrast, G3 mice from the outcross strategy described above are used both for screening and to assess chromosomal location, and their genetic background averages 62.5% from C3; the time from identification of a phenotype to a map location in this earlier study was 1.5 months. Approximately 70% of heritable phenodeviants in the outcross strategy were mapped because the phenotype was identified on a mixed background that contained segregating modifier genes.

Plasma collection and analysis

Blood samples from 9-week-, 11-week-, or 13-week-old animals were collected in EDTA plasma tubes using submandibular puncture of nonanesthetized mice following a 4 h fast. Blood glucose was immediately measured using a OneTouch Profile glucometer (LifeScan, Milpitas, CA). Plasma was stored at −80°C until it was thawed and analyzed. Total plasma cholesterol, HDL-cholesterol, and triglyceride levels were measured in frozen plasma using an Olympus AU400e Chemistry Analyzer (Olympus America, Inc., Center Valley, PA). Reagents for cholesterol and triglyceride measurements were purchased from Boehringer Mannheim Corp. (Indianapolis, IN). Plasma samples were collected and stored on ice, vortexed, and cleared by brief centrifugation.

Genome mapping

Genomic DNA was extracted from mouse tails using standard protocols. Genome-wide scans were performed using either the Mutation Mapping and Developmental Analysis Project's genotyping service at Harvard Medical School with the 768 SNP Illumina panel (24) or at Amgen with the Illumina Mouse Medium Density Linkage Panel (Illumina, San Diego, CA) consisting of 1,449 loci distributed at a density of approximately three single-nucleotide polymorphisms (SNPs) per 5 Mb interval. All reactions were performed according to the manufacturer's recommendations, and fluorescence signal was assayed using the Illumina BeadArray Reader and BeadScan v3.5. Control samples (B6 and C3) were included for each Sentrix Array Matrix or BeadChip hybridized. Loci with the same SNP call between the two control samples were excluded from analysis, and the remaining 939 informative loci were used to determine the parental lineage for SNPs in the experimental samples.

Individual marker genotyping

M13-tailed mouse primers for microsatellite loci *D7Mit76*, *D7Mit294*, *D7Mit266*, *D7Mit309*, *D3Mit212*, *D3Mit101*, *D3Mit75*, *D3Mit102*, *D3Mit215*, and *D3Mit42* were amplified using PCR and labeled by including M13-29 primer tagged with either IRD-700 or IRD-800 infrared dyes (LiCor, Lincoln, NE) in the reaction mixture. The products were resolved on denaturing polyacrylamide gels and detected with a LiCor GeneReadIR 4200 Gene Analyzer. Six SNPs were used for fine mapping, four on mouse chromosome 7 (*rs31742536*, *rs4135452*, *rs13479172*, and *rs3142570*), and two on mouse chromosome 3 (*rs13477318* and *rs13477320*). Forward and reverse primers were made based on the SNP sequences, and PCR reactions were set up using Expand Long Template PCR System (Roche Diagnostics Corp., Indianapolis, IN). PCR products were then gel purified and sequenced as described below.

TABLE 1. Plasma characteristics of the ENU screen of 7,546 9-week-old B6×C3 mice

Sex	Total Mice Screened	Weight[a]	Glucose	Cholesterol[a]	Triglyceride[a]	Leptin[a]	Insulin[a]
		g		*mg/dl*		*ng/ml*	
Males	3,818						
Mean ± SD		27.3 ± 3.5	128.6 ± 23.4	134.5 ± 34.3	163.6 ± 58.3	3.4 ± 5.0	1.4 ± 1.1
Median		27.1	128	130	155	2.2	1.2
Median ± 3 SD		19.2–38.2	61.3–194.7	64.9–260.5	58.1–415.9	0.1–31.3	0.2–6.6
Females	3,728						
Mean ± SD		22.0 ± 2.8	115.5 ± 19.9	111.8 ± 30.6	123.2 ± 45.2	2.2 ± 3.0	0.9 ± 1.2
Median		21.9	115	109	115	1.5	0.7
Median ± 3 SD		15.6–30.7	55.3–174.7	53.8–220.8	41.0–322.4	0.1–18.7	0.1–4.6

ENU, *N*-ethyl-*N*-nitrosourea.
[a] Statistical analyses and SD were calculated from log-transformed data.

Gene sequencing

Mouse genomic DNA sequences were obtained from the following published contigs: NT_039413 for mouse chromosome 7; NT_109315 for mouse chromosome 4; and NT_039240 for mouse chromosome 3. Forward and reverse primers for exons of genes of interest were designed in the intron regions so that sequencing would cover the entire exon. PCR reactions were set up as described above and gel purified. For sequencing, purified PCR products were used in a cycle sequencing reaction using BigDye 3.1 terminator kit (Applied Biosystems, Foster City, CA) according to the manufacturer's recommendations. Samples were then sequenced using an ABI3700 or an ABI3730 Genetic Analyzer (Applied Biosystems). DNA sequence data analysis was performed using SeQuencher program (Genecodes, Ann Arbor, MI).

Statistical identification of outliers

Measurements were made on each animal, consisting of weight, blood levels of glucose, total cholesterol, triglycerides, leptin, and insulin. Distributions of these measurements were found to be log-normal with the exception of glucose, which was normally distributed. After log-transformation as appropriate, the mean and standard deviation were estimated using the median absolute deviation method, which was robust to the presence of outliers in the data set (25). Each of the measurements was converted to a Z-score based on the mean and standard deviation estimated from the previous two weeks' data. Values from male and female animals were calculated separately. A significant outlier measurement was identified using a two-tailed test with an α threshold of 0.00625 (0.05/8 after applying a Bonferroni correction for multiple testing). Significant pedigrees were identified as having more than one animal in the analyzed pedigree with a significant outlier in the same measurement.

Protein analyses

Immunohistochemistry to detect CCAAT/enhancer binding protein α (C/EBPα) in formalin-fixed liver sections was carried out on deparaffinized tissue sections following antigen retrieval (Diva Decloaker RTU, Biocare Medical, Concord, CA). Tissue sections were blocked with CAS BLOCK (Zymed Laboratories, San Francisco, CA) and incubated with a rabbit anti-C/EBPα (14AA, Santa Cruz Biotechnology, Santa Cruz, CA). Tissue sections were quenched with Peroxidase Blocking Solution (Dako Corp., Carpenteria, CA) and detected with anti-rabbit-labeled polymer-HRP (Envision System+, Dako Corp.). Reaction sites were visualized with DAB+ Substrate-Chromagen System (DAKO Corp.) and counterstained with hematoxylin.

For Western blot analyses of ABCA1 protein, livers were homogenized in a glass Dounce homogenizer for 5 min in cold lysis buffer (10 mM Tris-HCl, pH 7.5, 150 mM NaCl, 0.5% Triton X-100, 0.5% sodium deoxycholate). Lysates were cleared by centrifuging at 4,400 *g* for 5 min at 4°C and were stored at −80°C with complete protease inhibitor (Roche Diagnostics Corp.). Samples containing 40 μg of protein were run on 12% SDS-PAGE Tris-glycine gels (Invitrogen, Carlsbad, CA), and Western blotting was carried out as previously reported (26).

RESULTS

A screen for ENU-induced recessive mutations affecting plasma biochemistry in G3 mice of mixed C3×B6 background

Cohorts of G3 mice were produced and bled at 9 weeks of age, resulting in the analysis of a total of 7,546 mice. These mice were progeny of 254 G1-pedigree founders, with a mean of 29.7 and a median of 29 G3 mice screened per founder. The phenotypic averages and ranges of body weight, blood glucose, plasma lipids (cholesterol and triglycerides), and metabolic hormones (insulin and leptin) are shown in **Table 1**. As expected, all six parameters were higher in male mice than in female mice. Using the statistical approach described in Materials and Methods, those mice with phenotypic values either below or above the range

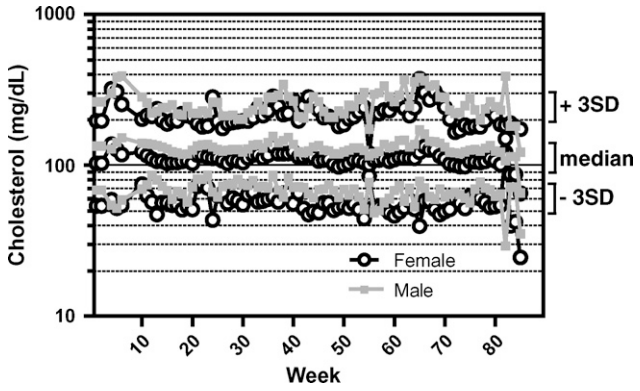

Fig. 1. Total cholesterol cutoffs for phenodeviant identification. The cholesterol median is shown for males (gray line) and females (black line) as a continually fluctuating statistic. During the course of the screen, the median and SD were calculated from phenotypic data of the 2 week period prior to the assay day (on average 100 mice of each sex). The raw cholesterol data were log transformed to generate normally distributed data, reflected by the log scale of the absolute cholesterol value of the median and outlier cutoff. Hypercholesterolemic and hypocholesterolemic mice were identified if they were >3 SD above or <3 SD below the median, respectively.

of the median ± 3 SD were considered as phenodeviants (Table 1). However, the 3 SD cutoffs shown in Table 1 are for all 7,546 analyzed mice; during the course of the screen, the actual criteria for flagging phenodeviants fluctuated with each weekly cohort. This was attributable to the statistical exclusion of data greater than 2 weeks prior to the assay for generating the cohort's median and SD to account for assay drift due to seasonal, handling, operator, or genetic background differences, as illustrated for plasma cholesterol (**Fig. 1A**) at 9 weeks. For example, the cutoff for male low-cholesterol phenodeviants ranged from 47.2 to 87.0 mg/dl (95% CI) and for high-cholesterol phenodeviants between 151.9 and 365.0 mg/dl (95% CI). Using this methodology, we observed three pedigrees of mice with low weight, and one pedigree with high insulin. We did not observe any

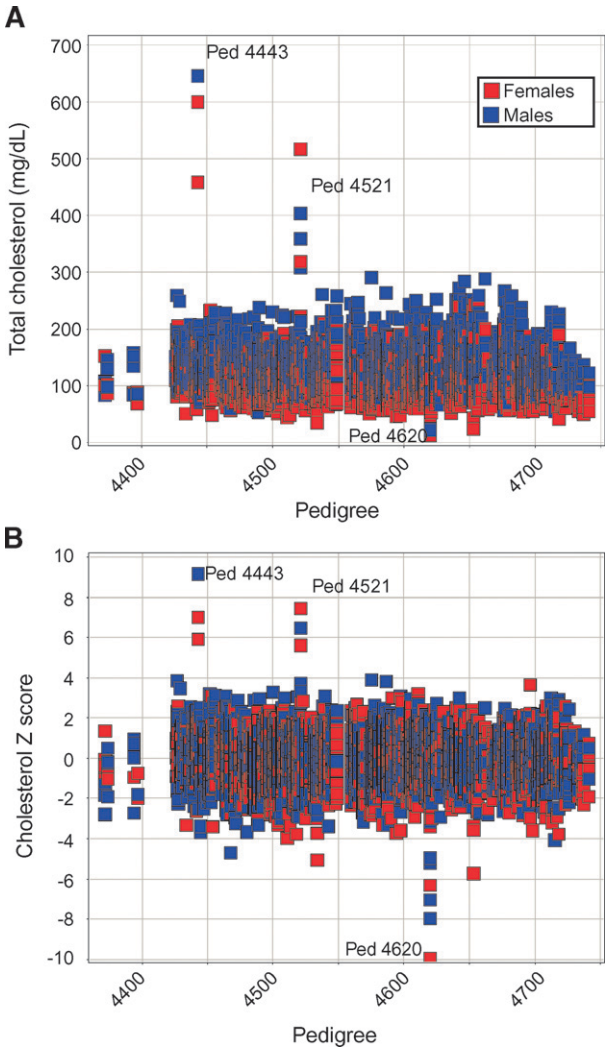

Fig. 2. Identification of three pedigrees of mice with cholesterol phenotypes. A: The individual cholesterol values of all 7,546 G3 mice screened are shown as separate squares for females (red) and males (blue). Phenotypic data are separated into pedigrees (*x* axis) and show three pedigrees containing mice with altered cholesterol values. Pedigrees (Ped) 4443 and 4521 exhibit hypercholesterolemic phenotypes, whereas pedigree 4620 exhibits a hypocholesterolemic phenotype. B: The data presented in A were converted to Z-scores and plotted similarly.

A

Marker	Mb	C3	B6	1	2	3	4
rs3695715	3.65	C	B	H	H	H	H
gnf04.002.008	5.01	C	B	H	H	H	H
gnf04.002.599	5.61	C	B	H	H	H	H
rs3660863	7.13	C	B	H	H	H	H
UT_4_10.84692	10.83	C	B	H	H	H	H
rs13477568	13.76	C	B	H	H	H	H
rs6287606	18.05	C	B	H	H	H	H
CEL-4_19508304	19.51	C	B	H	H	H	H
rs13477596	20.67	C	B	H	H	H	H
gnf04.019.134	22.31	C	B	H	H	H	H
rs3701432	29.49	C	B	H	H	H	H
rs3663744	31.22	C	B	H	H	H	H
rs3674908	32.44	C	B	H	H	H	H
rs13477643	35.07	C	B	H	H	H	H
rs3684104	38.41	C	B	H	H	H	H
rs13477662	39.88	C	B	H	H	H	H
CEL-4_40541402	40.54	C	B	H	H	H	H
rs3698283	42.43	C	B	H	H	H	B
rs13477681	45.42	C	B	H	H	H	B
rs3676423	51.04	C	B	B	B	B	B
rs13477709	52.68	C	B	B	B	B	B
rs3677770	53.96	C	B	B	B	B	B
rs6239799	55.77	C	B	B	B	B	B
rs3712541	59.10	C	B	B	B	B	B
rs3690581	61.03	C	B	B	B	B	B
rs3711477	84.51	C	B	B	H	H	B
rs6209043	88.27	C	B	B	H	H	B
rs13477838	89.45	C	B	B	H	H	B
rs3659791	94.28	C	B	B	H	H	B
rs13477873	99.78	C	B	B	H	H	B
rs6315002	101.40	C	B	B	H	H	B
rs13477883	102.31	C	B	B	H	H	B
rs6324470	104.32	C	B	B	H	H	B
rs6226080	107.06	C	B	B	H	H	B
rs3709486	109.97	C	B	B	H	H	B
rs6381371	114.38	C	B	B	H	H	B
rs3692563	116.74	C	B	B	H	H	B
rs3675629	119.40	C	B	B	H	H	B
rs13477952	121.32	C	B	B	H	H	B
rs13477959	122.57	C	B	B	H	H	B
rs13477965	125.08	C	B	B	H	H	B
gnf04.123.367	126.40	C	B	B	H	H	H
rs6355837	128.08	C	B	B	H	H	H
UT_4_132.137715	131.71	C	B	B	H	H	H
rs13478002	135.13	C	B	B	H	H	H
rs4224864	136.66	C	B	B	H	H	H
rs3688566	140.03	C	B	B	H	H	H
rs3719891	140.96	C	B	B	H	H	H
rs6230717	145.79	C	B	B	H	H	H
rs13478089	152.32	C	B	H	C	H	H
rs13478068	153.10	C	B	H	C	H	H
rs6279100	154.07	C	B	H	C	H	H

B

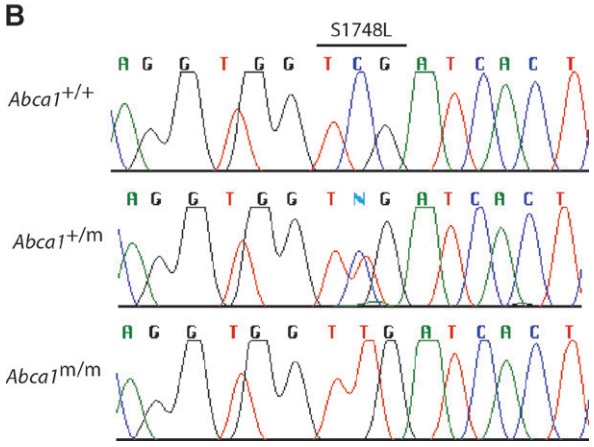

Fig. 3. Mapping the hypocholesterolemic phenotype in pedigree 4620. A: Four mice with hypocholesterolemia were used for genome scan analysis. Haplotypes for chromosome 4 are shown for the individual mice and for a B6 and C3 mouse to identity informative SNPs; homozygous C3 (C-blue), heterozygous (H-yellow), and homozygous B6 (B-red) alleles are shown for each marker. The minimal inherited B6 locus is shown by the bolded black box. B: Chromatographs of *Abca1* in wild-type *Abca1*$^{+/+}$, heterozygous *Abca1*$^{+/m}$, and hypocholesterolemic *Abca1*$^{m/m}$ mice. Mutation at codon 1,748 results in a serine-to-leucine missense mutation.

families of mice with either high or low glucose; in fact, only one mouse with a blood glucose >250 mg/dl was observed in the entire group of 7,546 mice.

Identification of plasma lipid phenodeviants

We identified three pedigrees of mice with significant outliers for plasma cholesterol levels (**Fig. 2A, B**). The outliers from the pedigrees were all clearly >5 SD from the medians of the populations (Fig. 2B). Mice from pedigrees 4443 and 4521 were identified with very high levels of total plasma cholesterol. Pedigree 4443 mice had higher levels of cholesterol than those in pedigree 4521. Mice from pedigree 4620 exhibited very low total cholesterol. We observed that some hypercholesterolemic mice also had high circulating triglyceride levels (see below). No changes in the other tested serum parameters were observed in mice from these three pedigrees nor were any behavioral or grossly visible phenotypes. Inheritance of the phenotypes was confirmed in G3 offspring from rematings of relevant G2×G1 parents and in subsequent generations for mice of both sexes in all three pedigrees.

Identification of a mutation in *Abca1* in the hypocholesterolemic pedigree 4620

A genome scan on the first four mice with very low levels of plasma cholesterol from pedigree 4620 revealed a single region of homozygosity for B6 on chromosome 4 (**Fig. 3A**); this was the only locus that was homozygous in all four affected mice. This region spanned 39.1 Mb, but contained the strong candidate gene *Abca1*. In mice with the low-cholesterol-levels phenotype, sequencing of all the exons from the *Abca1* gene revealed a cytosine-to-thymine transition within exon 10. This transition resulted in a missense alteration of serine to leucine at residue 1,748 in the protein (Fig. 3B). Expansion of the pedigree showed that homozygosity for the mutation and low-cholesterol phenotype cosegregated in mice of both sexes. Homozygosity for $Abca1^{S1748L}$ (designated $Abca1^{m}$ for simplicity) led to severe reduction of total plasma cholesterol, and intermediate cholesterol levels were seen in heterozygous mice (**Fig. 4A**). A significant increase in triglycerides was seen in $Abca1^{m}$ homozygous mice, but not in heterozygous mice (Fig. 4B). For all three genotypes, a clear correlation was observed between total cholesterol and HDL-cholesterol levels (Fig. 4C), demonstrating that the mutation impacted the level of HDL-cholesterol. Also, the plasma cholesterol levels phenotypes were 100% penetrant in $Abca1^{m/m}$ mice from both sexes, confirmed by consecutive bleeds performed at 11 and 13 weeks of age. The semi-dominance for cholesterol (total and HDL) levels of the *Abca1* allele was supported with hepatic ABCA1 protein levels as shown by Western blots (Fig. 4D).

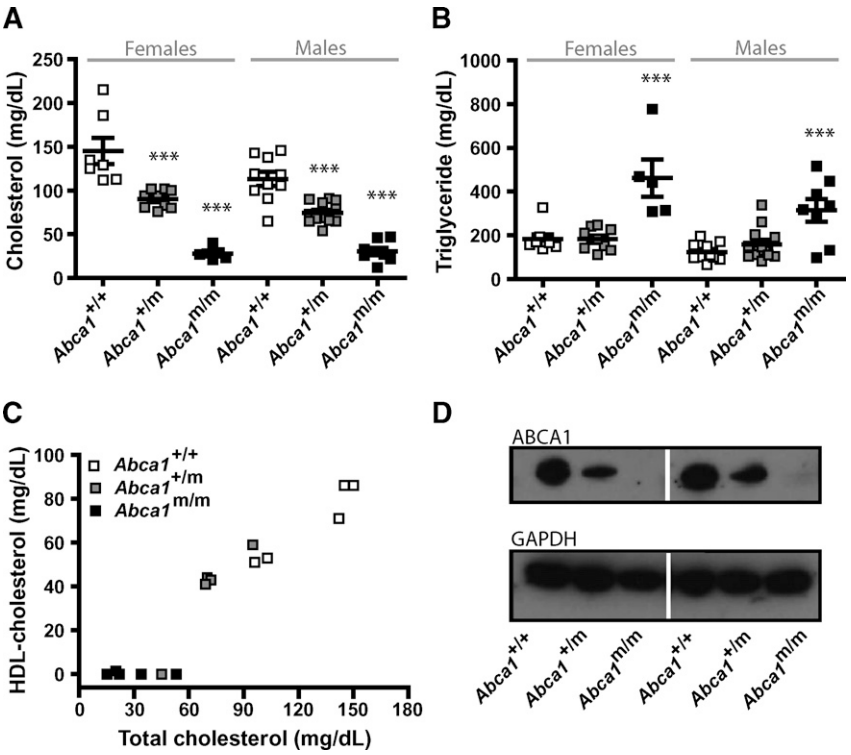

Fig. 4. Phenotypic characterization of $Abca1^{m/m}$ mice. Plasma total cholesterol (A) triglyceride (B), and HDL-cholesterol (C) were analyzed in 11-week-old fasted mice. Mice of both sexes were segregated as wild-type ($^{+/+}$), heterozygous ($^{+/m}$), and homozygous mutant *Abca1* ($^{m/m}$). D: Expression of ABCA1 protein was analyzed in liver homogenates from several mice of each genotype. All data points represent the phenotypic value from individual mice; mean and SEM are shown by the bars within a column. Statistical analyses were carried out by one-way ANOVA using a Tukey posthoc test. *** $P < 0.0001$ versus wild-type sex-matched mice.

Identification of a mutation in *Cebpa* in the hypercholesterolemic pedigree 4443

Three cholesterol outliers were identified among 31 G3 mice in two of five families from pedigree 4443 (Fig. 2A). The offspring of these two families yielded additional affected hypercholesterolemic mice. These animals were utilized to map the causative gene to chromosome 7 using SNP analysis as shown in **Fig. 5A**. This region contained the *Apoe* cluster of genes, which automatically became candidate genes. *Apoc2*, *Apoc4*, *Apoc1*, and *Apoe* genes were sequenced, but no mutations were found. Microsatellite markers and SNP analysis were used to screen for mice containing crossovers within the interval. This analysis allowed us to reduce the region of interest to 11.1 Mb, from *rs4135452* (26.0 Mb) to *D7Mit309* (37.1 Mb), and excluded the *Apoe* locus (data not shown). There are total of 185 annotated genes within this region, and 46 genes were chosen and sequenced, revealing a single-nucleotide alteration. A thymine-to-adenine transversion was identified in the single exon of the *Cebpa* gene (encoding C/EBPα; Fig. 5B). At the protein level, this results in a missense mutation of isoleucine to asparagine at amino acid 68. Following the genotyping of the mutation in 385 mice in the pedigree, the frequency of affected mice was below the total number of observed homozygous mutant *Cebpa*^{m} mice, indicative of reduced penetrance. In addition, a complicating factor in confirming the mutation in *Cebpa* as underlying the phenotype was the infrequent occurrence of hypercholesterolemic mice that were heterozygous for the mutation at this locus. Recombinants between *rs142570* and *Cebpa* were identified (Fig. 5C, top haplotype) and intercrossed to produce 21 mice that were homozygous for the B6 haplotype, including *D7Mit76* and *rs142570*, and homozygous for the C3 haplotype, which included wild-type *Cebpa* and *D7Mit309* (Fig. 5C, bottom haplotype). None of the mice homozygous for the wild-type C3 *Cebpa* allele were affected. Thus, mutation in *Cebpa* was required for the hypercholesterolemic phenotype; however, the interval between *rs3142570* and *Cebpa* could not be excluded as a region potentially harboring an additional mutation.

Genotyping for the I68N mutation was carried out in 385 of the 466 mice generated in the pedigree to assess penetrance. The affected phenotype was extremely variable, and mice were classified as affected when plasma cholesterol levels were outside the range seen in *Cebpa*$^{+/+}$ wild-type mice for any one of the three independent blood collections (see supplementary Table I). Only 53 of the 84 male mice homozygous for *Cebpa*^{m} were affected, lead-

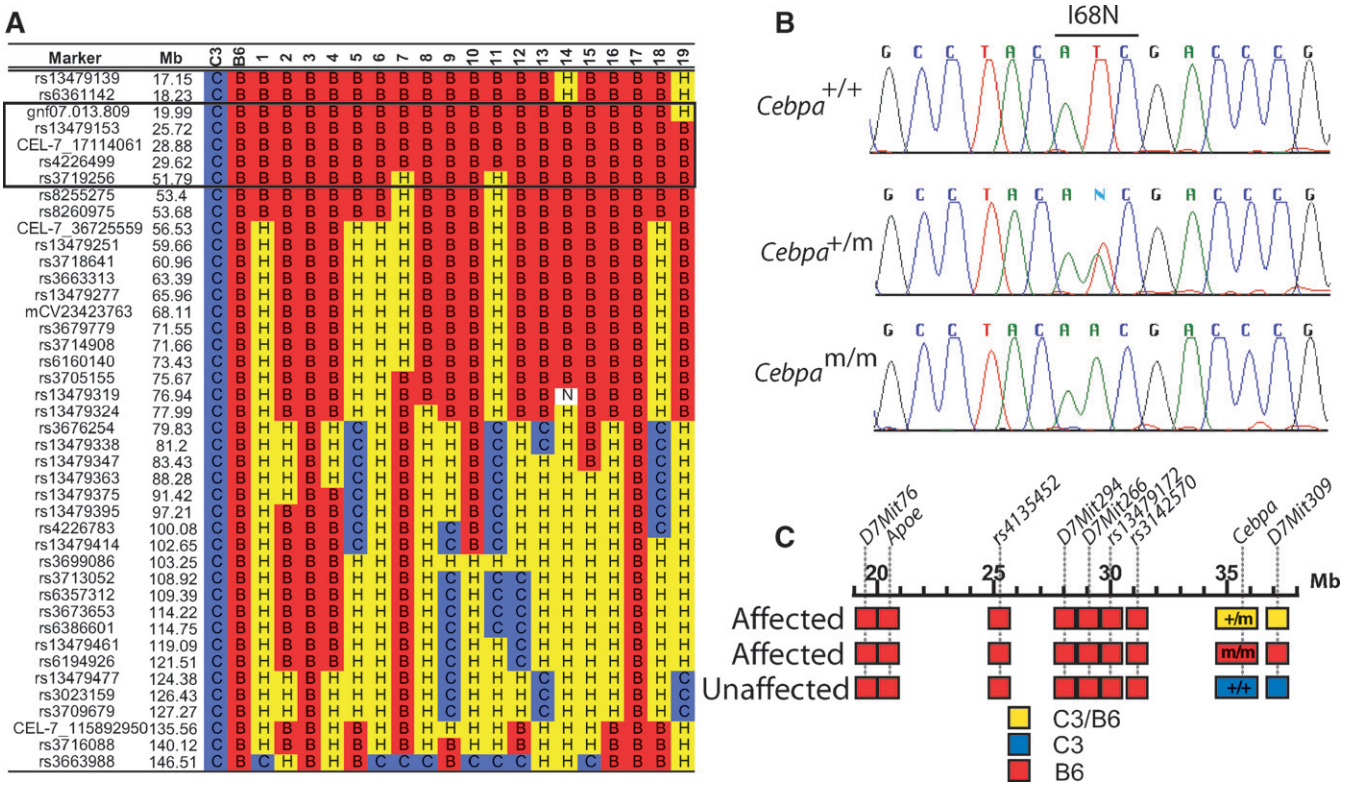

Fig. 5. Mapping of the hypercholesterolemic phenotype in pedigree 4443. A: Nineteen mice with hypercholesterolemia were used for genome scan analysis. Haplotypes for chromosome 7 are shown for all 19 mice and for a B6 and C3 mouse to identify informative SNPs; homozygous C3 (C-blue), heterozygous (H-yellow), and homozygous B6 (B-red) alleles are shown for each marker. The minimal inherited B6 locus is shown by the bolded black box. B: Chromatographs of *Cebpa* in wild-type *Cebpa*$^{+/+}$, heterozygous *Cebpa*$^{+/m}$, and hypercholesterolemic *Cebpa*$^{m/m}$ mice. Mutation at codon 68 results in an isoleucine-to-asparagine missense mutation. C: Recombinant analysis identified an affected heterozygous *Cebpa*$^{+/m}$ mouse (top haplotype) and is compared with an affected hypercholesterolemic *Cebpa*$^{m/m}$ mouse (middle haplotype). Backcrossing of the recombinant haplotype identified in the affected heterozygous *Cebpa*$^{+/m}$ mouse led to the identification of 21 mice exhibiting the bottom wild-type *Cebpa* haplotype, of which none were affected.

ing to a calculated penetrance of 63.1%; in female mice, the penetrance was only 41.9% (see supplementary Table I). Assessing penetrance was further complicated by the observation that the phenotype was labile in individual mice sampled at 9, 11, and 13 weeks (see supplementary Table I and **Fig. 6A–F**). For example, a *Cepba*$^{m/m}$ mouse hypercholesterolemic at 9 weeks could be normal at 11 weeks, or vice versa. Analysis of plasma from 11-week-old *Cebpa*$^{m/m}$ mice revealed high triglyceride as well as high cholesterol levels (**Fig. 7A, B**). In these mice, lipoprotein analysis showed strong elevation of HDL-cholesterol levels with a minimal increase in LDL-cholesterol and no change in VLDL-cholesterol levels (data not shown). This phenotype was evident, as shown in Fig. 7C; *Cebpa*$^{m/m}$ mice with high cholesterol levels also had high HDL-cholesterol levels. Notably, *Cebpa*$^{m/m}$ mice had slightly reduced body weights and some were runted (Fig. 7D, body weights <15 g). Interestingly, these mice with low body weight did not have high cholesterol levels. To determine whether the amino acid change in the pedigree 4443 mice resulted in altered C/EBPα protein expression, we performed immunohistochemistry on liver sections from *Cebpa*$^{m/m}$ mice and wild-type *Cebpa*$^{+/+}$ controls (Fig. 7E). No differences were detected in the level of expression or the typical nuclear localization of C/EBPα between *Cebpa*$^{+/+}$ and *Cebpa*$^{m/m}$ mice.

Mapping of the hypercholesterolemic mutation in pedigree 4521 to chromosome 3

Finally, the second hypercholesterolemic pedigree (4521) of mice was expanded to produce a large extended family of 435 animals. A genome scan analysis of the animals with the affected phenotype revealed a consistently inherited B6 region on chromosome 3 (**Fig. 8A**). Genotyping of microsatellite markers was carried out to refine this minimal B6 region to 7 Mb (Fig. 8B) in affected mice. This interval contained 131 genes (and expressed sequence tags), of which none were obvious functional candidates. To segregate the animals for phenotypic characterization, mice were separated based on the haplotype of the markers between *D3Mit214* and *rs13477318*, a region that encompasses the causative locus (referred to as B6^{m}). When

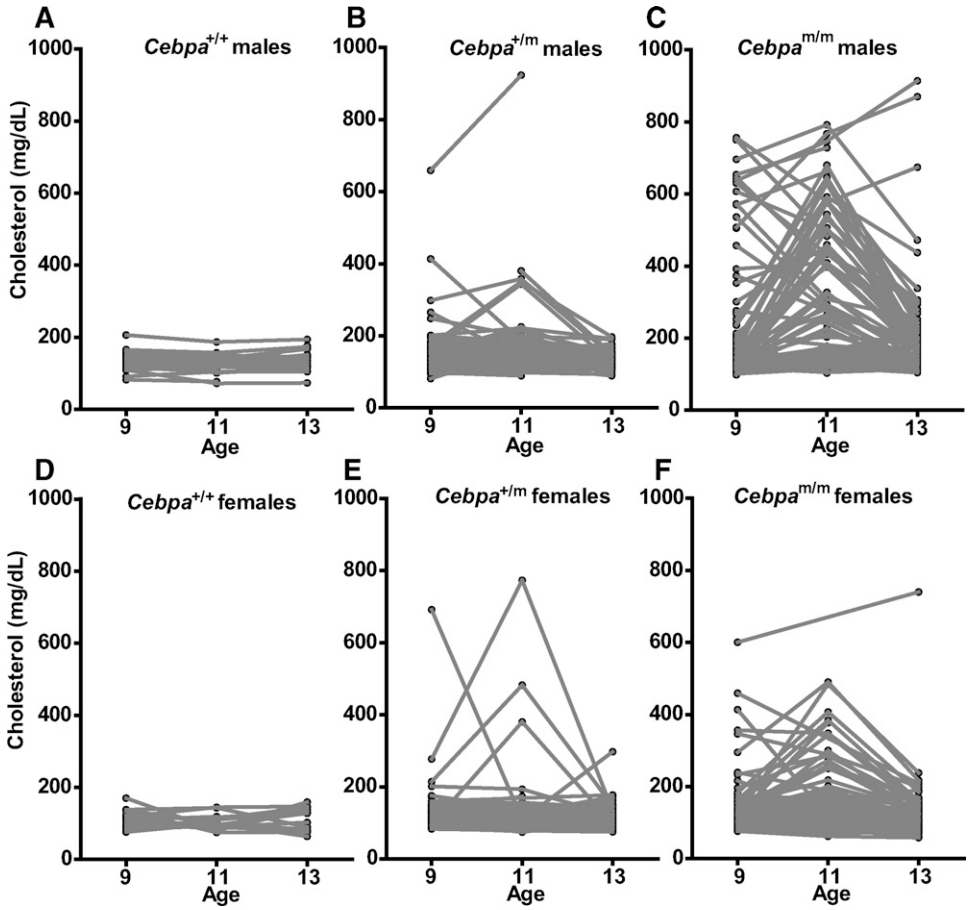

Fig. 6. Assessment of the penetrance and labile phenotype in *Cebpa*$^{m/m}$ mice. Plasma total cholesterol was assessed in mice at three test ages (9, 11, or 13 weeks). *Cebpa* mice of both sexes were analyzed. A, D: Wild-type ($^{+/+}$); B, E: heterozygote ($^{+/m}$), and C, F: homozygote mutant *Cebpa* ($^{m/m}$) mice. Cholesterol levels in wild-type *Cebpa*$^{+/+}$ mice were stable and not elevated, whereas cholesterol levels in homozygous mutant *Cebpa*$^{m/m}$ mice ranged widely and fluctuated from one time point to another. All data points represent the phenotypic value from individual mice, and the lines connect the values from the same mouse. In some cases, values were not gathered for every mouse at every time point.

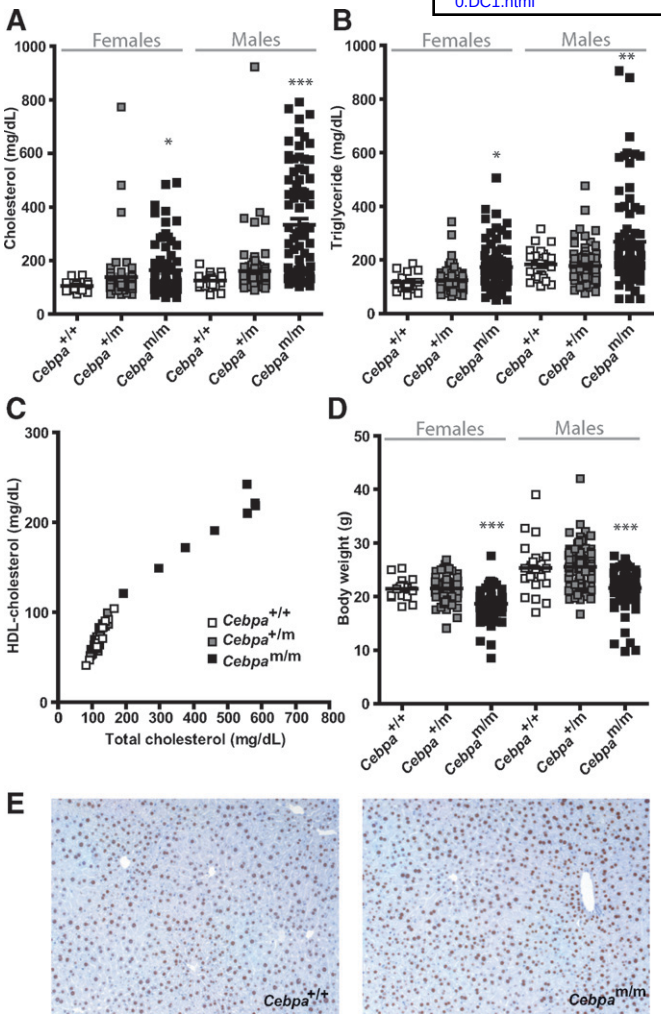

Fig. 7. Phenotypic characterization of *Cebpa*$^{m/m}$ mice. Plasma total cholesterol (A), triglyceride (B), HDL-cholesterol levels (C), and body weight (D) were analyzed in 11-week-old fasted mice. Mice of both sexes were segregated as wild-type ($^{+/+}$), heterozygous ($^{+/m}$), and homozygous mutant *Cebpa* ($^{m/m}$). All data points represent the phenotypic value from individual mice; mean and SEM are shown by the bars within a column. Statistical analyses were carried out by one-way ANOVA using a Tukey posthoc test. * $P < 0.05$, ** $P < 0.01$, *** $P < 0.0001$ versus wild-type sex-matched mice. E: Expression of C/EBPα protein was analyzed by immunohistochemistry in liver sections from wild-type *Cebpa*$^{+/+}$ and *Cebpa*$^{m/m}$ mice. Immunoreactive C/EBPα was detected with DAB+ substrate (brown), and slides were counterstained with hematoxylin (blue).

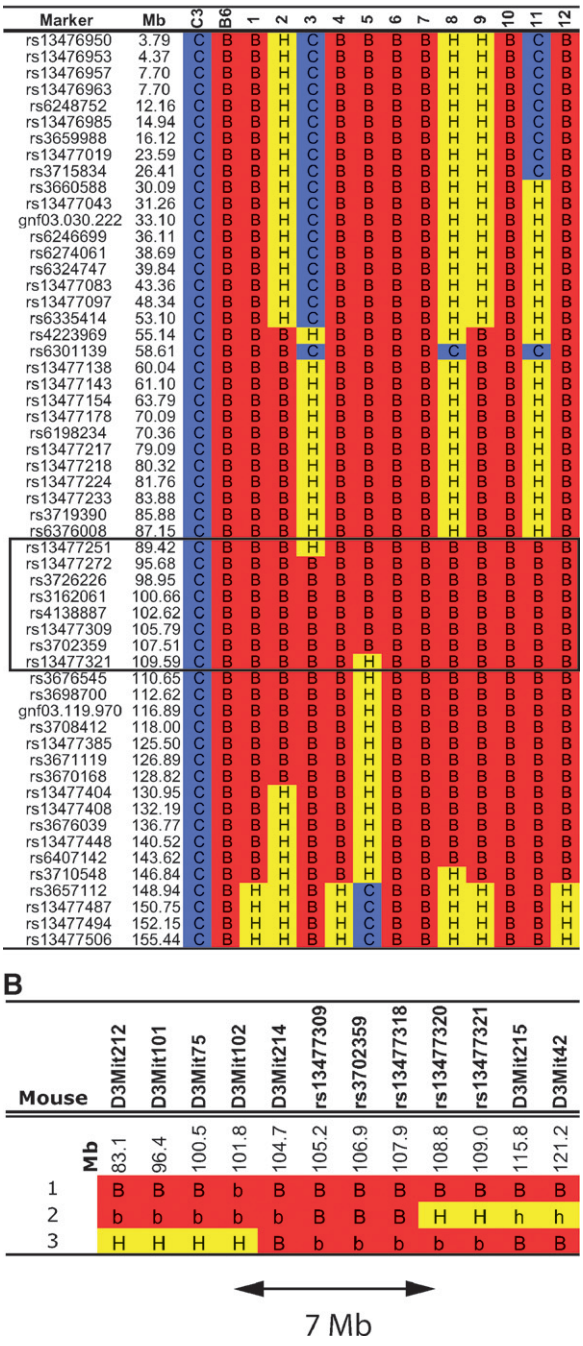

Fig. 8. Mapping of the hypercholesterolemic phenotype in pedigree 4521. A: Twelve mice with hypercholesterolemia were used for genome scan analysis. Haplotypes for chromosome 3 are shown for the individual mice and for a B6 and C3 mouse to identify informative SNPs; homozygous C3 (C-blue), heterozygous (H-yellow), and homozygous B6 (B-red) alleles are shown for each marker. The minimal inherited B6 locus identified by genome scan analyses is shown by the bolded black box. B: Fine mapping of the B6 locus in three additional mice with hypercholesterolemia. Polymorphic SNPs and microsatellites were typed in recombinant mice to fine map the recombination. The refined B6 locus is shown by the double arrow. Alleles in lower case are inferred from flanking markers and/or parental genotypes.

mice were divided by sex and genotype, their cholesterol values at the three tested ages (9, 11, and 13 weeks) were plotted and revealed similarities with the *Cebpa*$^{m/m}$ mice (**Fig. 9A–F**). First, hypercholesterolemia was not fully penetrant in B6$^{m/m}$ mice, and second, the phenotype of affected mice was labile. The phenotype was most obvious at 9 weeks of age (particularly in female B6$^{m/m}$ mice), but could return to normal levels at later tested ages (Fig. 9C). This trend was slightly different in male B6$^{m/m}$ mice; many males retained the affected phenotype at 11 and 13 weeks of age (Fig. 9F). At 9 weeks of age, the calculated penetrance was 81.8% for males and 53.7% for females (see supplementary Table II). However, the overall penetrance

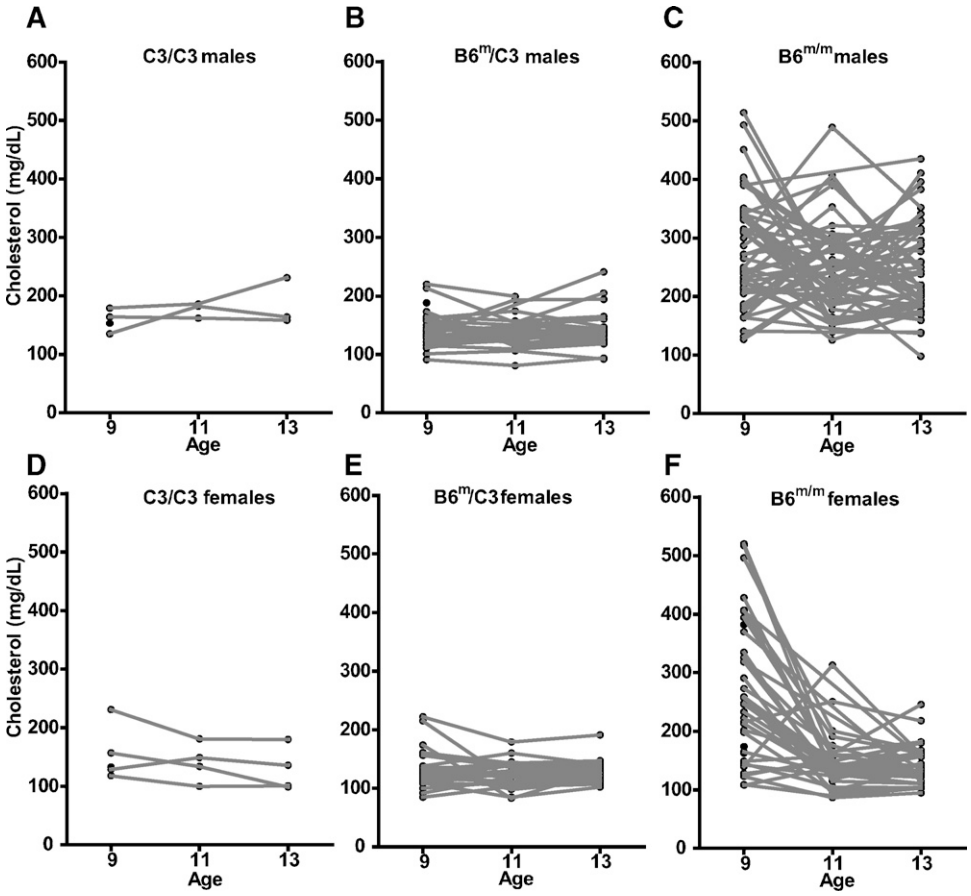

Fig. 9. Assessment of the penetrance and labile phenotype in pedigree 4521 mice mapped to chromosome 3. Plasma total cholesterol levels were assessed in mice at three different ages (9, 11, or 13 weeks). Mice from pedigree 4521 were segregated at the chromosome 3 locus based on the haplotype between markers *D3Mit214* and *rs13477318* as homozygous mutants ($B6^{m/m}$), heterozygotes ($B6^{m}/C3$), or C3 homozygotes (C3/C3). Mice from both sexes were analyzed. A, D: C3/C3; B, E: $B6^{m}/C3$; and C, F: $B6^{m/m}$. Cholesterol levels in mice C3 homozygous for the haplotype on chromosome 3 were stable and not elevated (A, D); whereas cholesterol levels in the mice homozygous $B6^{m/m}$ ranged widely and fluctuated from one age to another. All data points represent the phenotypic value from individual mice, and the lines connect the values from the same mouse. In some cases, not all values were gathered for every mouse at every time point.

(animals that had cholesterol levels higher than wild-type C3/C3 mice at any of the tested ages) for males and females was 98.5% and 63.0%, respectively. In contrast to the $Cebpa^{+/m}$ mice, there was no evidence of semi-dominance; all $B6^{m}/C3$ mice were unaffected. Only homozygous $B6^{m}$ mice exhibited very high levels of total cholesterol (Figs. 9C, F, **10A**), with occasional hypertriglyceridemia (Fig. 10B). Further, the increase in total cholesterol levels correlated with an increase in HDL-cholesterol levels (Fig. 10C). $B6^{m/m}$ mice had slightly lower body weights (Fig. 10D), but were otherwise healthy and exhibited no other overt phenotypes.

DISCUSSION

The biochemical screening of plasma from mutagenized families of mice has permitted the identification of many pedigrees of mice with either high or low HDL-cholesterol levels. Eighteen hypocholesterolemic (27–29) and nine hypercholesterolemic (30) families of mice from ENU mutagenesis screens have been described in the literature to date. However, genetic mapping and the identification of a causative mutation was only carried out in one family, revealing a mutation in *Lcat* (29). In light of this, we set out to identify pedigrees of mice with metabolic plasma biochemical traits, including altered cholesterol phenotypes, using ENU mutagenesis, and engaged an outcross strategy aimed at facilitating gene identification. We identified three inherited alleles of HDL-cholesterol and lipid phenotypes using a recessive screen. Two of these alleles are linked to mutations in the *Abca1* and *Cebpa* genes with the phenotypes of low and high HDL-cholesterol, respectively. The third allele allowed us to identify a novel locus on chromosome 3 that confers a high HDL-cholesterol phenotype.

In the current study, mice heterogeneous for B6 and C3 were screened to select for robust phenotypes and advance mapping efforts. Surprisingly, no families of mice with glucose phenotypes were observed, and only one potential insulin phenotype. Nevertheless, three lipid phenotypes

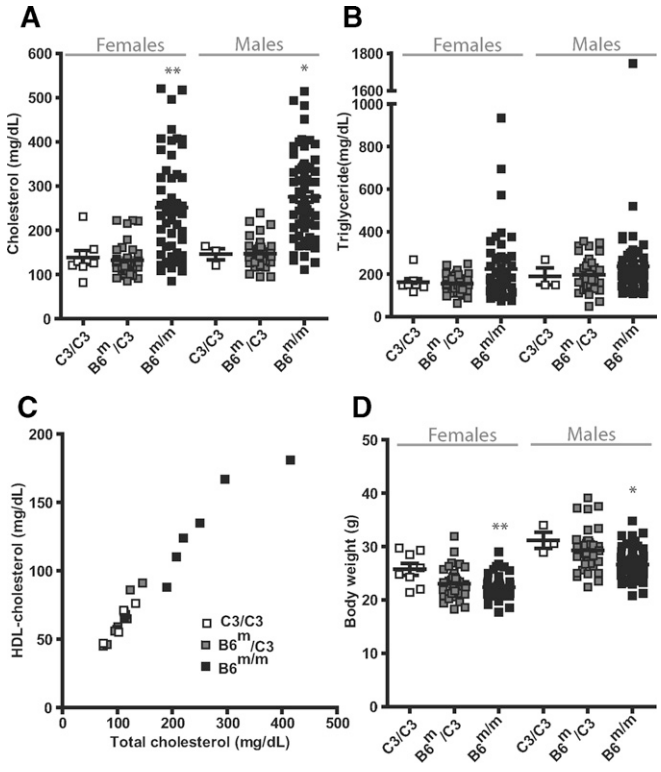

Fig. 10. Phenotypic characterization of the pedigree 4521 mice mapped to chromosome 3. Plasma total cholesterol (A), triglyceride (B), HDL-cholesterol levels (C), and body weight (D) were analyzed in 9-week-old fasted mice. Mice from pedigree 4521 were segregated as described in Fig. 8. $B6^{m/m}$ mice had high total and HDL-cholesterol levels, with rare hypertriglyceridemia. All data points represent the phenotypic value from individual mice; mean and SEM are shown by the bars within a column. Statistical analyses were carried out by one-way ANOVA using a Tukey posthoc test. * $P < 0.05$, ** $P < 0.01$, versus wild-type sex-matched mice.

were identified. Interestingly, other HDL phenotypes produced by mutagenesis have also been established on either B6×C3 hybrid or C3 inbred backgrounds, potentially indicating that these genomes and combinations thereof are well suited for the identification of monogenic lipid traits (27, 29, 30).

Genetic background can have dramatic effects on lipid and cholesterol levels and induced phenotypes. For example, differences between inbred strains of mice allowed mapping of QTL affecting HDL-cholesterol levels (31). Similarly, the effects of a null allele of *Apoe* varied dramatically when expressed on different genetic backgrounds (32). Thus, it is not surprising that similar genetic effects could result in the reduced penetrance seen for two of the three loci that we identified, given the mixed genetic background of our G3 mice and subsequent generations. Crosses to produce congenic strains on the C3 and B6 backgrounds could potentially lead to identification of modifier loci. Less easy to explain is the curious observation of extreme fluctuations in HDL-cholesterol levels in the affected hypercholesterolemic animals. In contrast to the stable hypocholesterolemic phenotype in the *Abca1* homozygous mutant mice as assessed at the same bleeds at the three ages (data not shown), the hypercholesterolemic mice are unpredictable and their phenotype unstable. The processes underlying these changes are unknown but could be explained by a compensatory mechanism initiated by liver cholesterol transporters, for example. High levels of circulating HDL might lead to SR-BI upregulation in an attempt to lower cholesterol (33). Alternatively, the expression of an HDL remodeling factor such as endothelial lipase (EL) could be altered and could rapidly change HDL-cholesterol levels. Along these lines, it has been observed that HDL-cholesterol can increase by up to 46% within only 48 h in mice injected with an anti-EL antibody (34). These postulated compensatory effects may be different between the B6 and C3 strains. Thus, it is possible that the mixed genetic background not only influences penetrance but additionally interferes with phenotype expressivity. Further studies to monitor these rapid phenotypic changes alongside possible microarray analyses in congenic backgrounds are warranted.

The S1748L mutation in *Abca1* recapitulates the phenotype observed in knockout mice (35–37). It results in dramatically reduced ABCA1 protein levels (Fig. 4D), and is expected to impair cholesterol efflux, the first stage of reverse cholesterol transport. Although three complete knockouts have been independently generated (35–37), this is the first identification of either a spontaneous or an induced mouse mutation in this gene. Although the phenotype observed in S1748L mutant mice is very similar to that of the knockouts, we observed a minimal amount of protein. The mutation itself would not be expected to cause truncated or mis-spliced protein, but perhaps it may lead to a misfolded molecule detected and degraded by the intrinsic cellular quality control process (38). Alternatively, the mature protein could be unstable and could be removed from the cell. The S1748L mutation is predicted to be located in a transmembrane domain between the V1704D and N1800H missense mutations identified in patients with Tangier disease (39). Although 44 missense mutations have been identified in ABCA1, only 2 (W840R and V1704D) are expected to lie in the transmembrane domain. Thus, the mutation we identified here is unique in location within the polypeptide, and provides a new genetic mouse model of ABCA1 deficiency, which may be dissimilar to a complete knockout.

The mutation in C/EBPα is perhaps more intriguing. C/EBPα is a b-Zip transcription factor and an established master regulator of many cellular functions (40). In humans, it leads to acute myeloid leukemia when mutated, owing to the dominant-negative effect of the mutant proteins, blocking normal granulopoiesis (41). The knockout mouse dies postnatally, owing to a lack of induction of gluconeogenic enzymes (42). Furthermore, C/EBPα regulates adipogenesis in vitro (40), and is crucial for normal adipose tissue development, additionally confirmed in the knockout mice (42). However, it is not clear how the I68N mutation in C/EBPα could lead to the hypercholesterolemic HDL phenotype we observed. None of the expected phenotypes found in the knockout mice were seen in mice with the C/EBPα mutation. For example, granulocytes from

Cebpa$^{m/m}$ mice were not different compared with those from wild-type mice (data not shown). Also, no hypoglycemia following an extended 12 h fast was noticed, as might be expected if gluconeogenesis were perturbed (data not shown). However, some *Cebpa*$^{m/m}$ mice were very small (Fig. 4D), and also exhibited very low levels of leptin (data not shown), suggesting a defect in adipogenesis. Previously, only two reports have shown minimal differences in plasma cholesterol following in vivo manipulation of the *Cebpa* gene. In the first study, mice were generated that were deficient in hepatic C/EBPα; HDL-cholesterol was reduced in these animals and was associated with an increase in hepatic lipoprotein lipase (43). In the second study, postnatal depletion of C/EBPα led to reduced total cholesterol levels (44) and reduced expression of 3-hydroxy-3-methyl-glutaryl-CoA reductase. These two studies demonstrate that a loss-of-function allele of *Cebpa* can lead to reduced plasma (HDL) cholesterol. This contrasts with the phenotype we observed in *Cebpa*$^{m/m}$ mice, thus suggesting a gain-of-function effect of the I68N mutation. It is possible that this mutation has altered expression of a gene(s) that modulates HDL-cholesterol levels, either through decreased catabolism of HDL or through increased peripheral cholesterol efflux into HDL. Because of the lack of a pathogenic mechanism, we cannot exclude the possibility of an undetected linked mutation in a neighboring gene that leads to the phenotype in 4443 mice. If the mutation in *Cebpa* is indeed causative, the forward genetics approach that we adopted here would have revealed a novel role for C/EBPα that would not have been exposed using conventional approaches to understanding gene function (i.e., by knocking out the gene). Interestingly, a recent study in human subjects revealed a positive correlation between the expression level of adipose C/EBPα and HDL-cholesterol levels, and an association of a C/EBPα SNP with triglyceride levels, reinforcing the pathogenic link of C/EBPα and circulating lipids in both mice and humans (45).

Finally, the mapping of the second hypercholesterolemic phenotype identified a novel locus on chromosome 3 for HDL-cholesterol. To our knowledge, no previous study has reported linkage or association of this locus to an HDL phenotype in mice (13). Of the 131 candidate genes in the 7 Mb locus, none present ready hypotheses to lead to high HDL levels. Interestingly, recent GWA studies of humans have identified the corresponding region for plasma lipid levels (16). Variation in LDL-cholesterol is associated with a locus including the genes *SORT1*, *PSRC1*, and *CELSR2*. These three genes are contained within the minimal locus we identified in these mice. However, it is unclear whether the underlying genetic factor is responsible for the cholesterol variations in both these mutant mice and humans, because the lipoprotein species is different, namely LDL-cholesterol in the GWA studies, and HDL-cholesterol in the pedigree 4521 mice.

In summary, we have conducted an ENU mutagenesis screen and identified and mapped three HDL-cholesterol phenotypes. We successfully identified mutations in *Cebpa* and *Abca1* and mapped the second high-HDL phenotype to a small region. This study demonstrates the effectiveness of ENU mutagenesis in identifying genes *1*) known to be involved in HDL metabolism (*Abca1*), *2*) known to regulate whole-body metabolism but not previously associated with HDL (*Cebpa*), and *3*) with a potentially novel function in influencing HDL levels. Future studies will be focused on identifying the causative mutation in the chromosome 3 hypercholesterolemia locus and establishing a mechanism for the elevation of HDL in both these mice and the *Cebpa* mutant mice.

The authors would like to thank Dr. Russ Cattley and Efrain Pacheco for immunohistochemistry help, Silvia Capon for plasma biochemical analysis, Derek Silvius for mouse colony maintenance, and Dr. Bill Richards for helpful discussion.

REFERENCES

1. Rader, D. J., and A. Daugherty. 2008. Translating molecular discoveries into new therapies for atherosclerosis. *Nature.* **451:** 904–913.
2. Libby, P. 2001. Managing the risk of atherosclerosis: the role of high-density lipoprotein. *Am. J. Cardiol.* **88:** 3N–8N.
3. Ohashi, R., H. Mu, X. Wang, Q. Yao, and C. Chen. 2005. Reverse cholesterol transport and cholesterol efflux in atherosclerosis. *QJM.* **98:** 845–856.
4. Castelli, W. P., R. J. Garrison, P. W. Wilson, R. D. Abbott, S. Kalousdian, and W. B. Kannel. 1986. Incidence of coronary heart disease and lipoprotein cholesterol levels. The Framingham Study. *J. Am. Med. Assoc.* **256:** 2835–2838.
5. Badimon, J. J., L. Badimon, and V. Fuster. 1990. Regression of atherosclerotic lesions by high density lipoprotein plasma fraction in the cholesterol-fed rabbit. *J. Clin. Invest.* **85:** 1234–1241.
6. deGoma, E. M., R. L. deGoma, and D. J. Rader. 2008. Beyond high-density lipoprotein cholesterol levels evaluating high-density lipoprotein function as influenced by novel therapeutic approaches. *J. Am. Coll. Cardiol.* **51:** 2199–2211.
7. Young, S. G., and C. J. Fielding. 1999. The ABCs of cholesterol efflux. *Nat. Genet.* **22:** 316–318.
8. Schamaun, O., B. Olaisen, T. Gedde-Dahl, Jr., and P. Teisberg. 1983. Genetic studies of an apoA-I lipoprotein variant. *Hum. Genet.* **64:** 380–383.
9. Akita, H., H. Chiba, K. Tsuchihashi, M. Tsuji, M. Kumagai, K. Matsuno, and K. Kobayashi. 1994. Cholesteryl ester transfer protein gene: two common mutations and their effect on plasma high-density lipoprotein cholesterol content. *J. Clin. Endocrinol. Metab.* **79:** 1615–1618.
10. Breckenridge, W. C., J. A. Little, P. Alaupovic, C. S. Wang, A. Kuksis, G. Kakis, F. Lindgren, and G. Gardiner. 1982. Lipoprotein abnormalities associated with a familial deficiency of hepatic lipase. *Atherosclerosis.* **45:** 161–179.
11. Henderson, H. E., Y. Ma, M. F. Hassan, M. V. Monsalve, A. D. Marais, F. Winkler, K. Gubernator, J. Peterson, J. D. Brunzell, and M. R. Hayden. 1991. Amino acid substitution (Ile194—-Thr) in exon 5 of the lipoprotein lipase gene causes lipoprotein lipase deficiency in three unrelated probands. Support for a multicentric origin. *J. Clin. Invest.* **87:** 2005–2011.
12. Gotoda, T., N. Yamada, T. Murase, M. Sakuma, N. Murayama, H. Shimano, K. Kozaki, J. J. Albers, Y. Yazaki, and Y. Akanuma. 1991. Differential phenotypic expression by three mutant alleles in familial lecithin:cholesterol acyltransferase deficiency. *Lancet.* **338:** 778–781.
13. Wang, X., and B. Paigen. 2005. Genetics of variation in HDL cholesterol in humans and mice. *Circ. Res.* **96:** 27–42.
14. Rigotti, A., B. L. Trigatti, M. Penman, H. Rayburn, J. Herz, and M. Krieger. 1997. A targeted mutation in the murine gene encoding the high density lipoprotein (HDL) receptor scavenger receptor class B type I reveals its key role in HDL metabolism. *Proc. Natl. Acad. Sci. USA.* **94:** 12610–12615.
15. Kathiresan, S., O. Melander, C. Guiducci, A. Surti, N. P. Burtt, M. J. Rieder, G. M. Cooper, C. Roos, B. F. Voight, A. S. Havulinna, et al. 2008. Six new loci associated with blood low-density lipoprotein cholesterol, high-density lipoprotein cholesterol or triglycerides in humans. *Nat. Genet.* **40:** 189–197.

16. Willer, C. J., S. Sanna, A. U. Jackson, A. Scuteri, L. L. Bonnycastle, R. Clarke, S. C. Heath, N. J. Timpson, S. S. Najjar, H. M. Stringham, et al. 2008. Newly identified loci that influence lipid concentrations and risk of coronary artery disease. *Nat. Genet.* **40:** 161–169.
17. Lusis, A. J., and P. Pajukanta. 2008. A treasure trove for lipoprotein biology. *Nat. Genet.* **40:** 129–130.
18. Chen, Y., J. Rollins, B. Paigen, and X. Wang. 2007. Genetic and genomic insights into the molecular basis of atherosclerosis. *Cell Metab.* **6:** 164–179.
19. Mamontova, A., S. Seguret-Mace, B. Esposito, C. Chaniale, M. Bouly, N. Delhaye-Bouchaud, G. Luc, B. Staels, N. Duverger, J. Mariani, et al. 1998. Severe atherosclerosis and hypoalphalipoproteinemia in the staggerer mouse, a mutant of the nuclear receptor RORalpha. *Circulation.* **98:** 2738–2743.
20. Meiner, V. L., C. L. Welch, S. Cases, H. M. Myers, E. Sande, A. J. Lusis, and R. V. Farese, Jr. 1998. Adrenocortical lipid depletion gene (ald) in AKR mice is associated with an acyl-CoA:cholesterol acyltransferase (ACAT) mutation. *J. Biol. Chem.* **273:** 1064–1069.
21. Cordes, S. P. 2005. N-ethyl-N-nitrosourea mutagenesis: boarding the mouse mutant express. *Microbiol. Mol. Biol. Rev.* **69:** 426–439.
22. Barbaric, I., S. Wells, A. Russ, and T. N. Dear. 2007. Spectrum of ENU-induced mutations in phenotype-driven and gene-driven screens in the mouse. *Environ. Mol. Mutagen.* **48:** 124–142.
23. Shedlovsky, A., J. L. Guenet, L. L. Johnson, and W. F. Dove. 1986. Induction of recessive lethal mutations in the T/t-H-2 region of the mouse genome by a point mutagen. *Genet. Res.* **47:** 135–142.
24. Moran, J. L., A. D. Bolton, P. V. Tran, A. Brown, N. D. Dwyer, D. K. Manning, B. C. Bjork, C. Li, K. Montgomery, S. M. Siepka, et al. 2006. Utilization of a whole genome SNP panel for efficient genetic mapping in the mouse. *Genome Res.* **16:** 436–440.
25. Kutner, M., C. J. Nachtsheim, J. Neter, and W. Li. 2005. Applied Linear Statistical Models. 5th edition. McGraw-Hill/Irwin, New York.
26. Kumar, R., D. McClain, R. Young, and G. A. Carlson. 2008. Cholesterol transporter ATP-binding cassette A1 (ABCA1) is elevated in prion disease and affects PrPC and PrPSc concentrations in cultured cells. *J. Gen. Virol.* **89:** 1525–1532.
27. Aigner, B., B. Rathkolb, M. Mohr, M. Klempt, M. Hrabe de Angelis, and E. Wolf. 2007. Generation of ENU-induced mouse mutants with hypocholesterolemia: novel tools for dissecting plasma lipoprotein homeostasis. *Lipids.* **42:** 731–737.
28. Hough, T. A., P. M. Nolan, V. Tsipouri, A. A. Toye, I. C. Gray, M. Goldsworthy, L. Moir, R. D. Cox, S. Clements, P. H. Glenister, et al. 2002. Novel phenotypes identified by plasma biochemical screening in the mouse. *Mamm. Genome.* **13:** 595–602.
29. Wiltshire, T., M. T. Pletcher, S. Batalov, S. W. Barnes, L. M. Tarantino, M. P. Cooke, H. Wu, K. Smylie, A. Santrosyan, N. G. Copeland, et al. 2003. Genome-wide single-nucleotide polymorphism analysis defines haplotype patterns in mouse. *Proc. Natl. Acad. Sci. USA.* **100:** 3380–3385.
30. Mohr, M., M. Klempt, B. Rathkolb, M. H. de Angelis, E. Wolf, and B. Aigner. 2004. Hypercholesterolemia in ENU-induced mouse mutants. *J. Lipid Res.* **45:** 2132–2137.
31. Wittenburg, H., M. A. Lyons, R. Li, U. Kurtz, X. Wang, J. Mossner, G. A. Churchill, M. C. Carey, and B. Paigen. 2006. QTL mapping for genetic determinants of lipoprotein cholesterol levels in combined crosses of inbred mouse strains. *J. Lipid Res.* **47:** 1780–1790.
32. Wang, S. S., W. Shi, X. Wang, L. Velky, S. Greenlee, M. T. Wang, T. A. Drake, and A. J. Lusis. 2007. Mapping, genetic isolation, and characterization of genetic loci that determine resistance to atherosclerosis in C3H mice. *Arterioscler. Thromb. Vasc. Biol.* **27:** 2671–2676.
33. Tsuruoka, H., W. Khovidhunkit, B. E. Brown, J. W. Fluhr, P. M. Elias, and K. R. Feingold. 2002. Scavenger receptor class B type I is expressed in cultured keratinocytes and epidermis. Regulation in response to changes in cholesterol homeostasis and barrier requirements. *J. Biol. Chem.* **277:** 2916–2922.
34. Jin, W., J. S. Millar, U. Broedl, J. M. Glick, and D. J. Rader. 2003. Inhibition of endothelial lipase causes increased HDL cholesterol levels in vivo. *J. Clin. Invest.* **111:** 357–362.
35. Christiansen-Weber, T. A., J. R. Voland, Y. Wu, K. Ngo, B. L. Roland, S. Nguyen, P. A. Peterson, and W. P. Fung-Leung. 2000. Functional loss of ABCA1 in mice causes severe placental malformation, aberrant lipid distribution, and kidney glomerulonephritis as well as high-density lipoprotein cholesterol deficiency. *Am. J. Pathol.* **157:** 1017–1029.
36. McNeish, J., R. J. Aiello, D. Guyot, T. Turi, C. Gabel, C. Aldinger, K. L. Hoppe, M. L. Roach, L. J. Royer, J. de Wet, et al. 2000. High density lipoprotein deficiency and foam cell accumulation in mice with targeted disruption of ATP-binding cassette transporter-1. *Proc. Natl. Acad. Sci. USA.* **97:** 4245–4250.
37. Orso, E., C. Broccardo, W. E. Kaminski, A. Bottcher, G. Liebisch, W. Drobnik, A. Gotz, O. Chambenoit, W. Diederich, T. Langmann, et al. 2000. Transport of lipids from golgi to plasma membrane is defective in tangier disease patients and Abc1-deficient mice. *Nat. Genet.* **24:** 192–196.
38. Vashist, S., and D. T. Ng. 2004. Misfolded proteins are sorted by a sequential checkpoint mechanism of ER quality control. *J. Cell Biol.* **165:** 41–52.
39. Brunham, L. R., R. R. Singaraja, and M. R. Hayden. 2006. Variations on a gene: rare and common variants in ABCA1 and their impact on HDL cholesterol levels and atherosclerosis. *Annu. Rev. Nutr.* **26:** 105–129.
40. Rosen, E. D. 2002. The molecular control of adipogenesis, with special reference to lymphatic pathology. *Ann. N. Y. Acad. Sci.* **979:** 143–158.
41. Nerlov, C. 2004. C/EBPalpha mutations in acute myeloid leukaemias. *Nat. Rev. Cancer.* **4:** 394–400.
42. Wang, N. D., M. J. Finegold, A. Bradley, C. N. Ou, S. V. Abdelsayed, M. D. Wilde, L. R. Taylor, D. R. Wilson, and G. J. Darlington. 1995. Impaired energy homeostasis in C/EBP alpha knockout mice. *Science.* **269:** 1108–1112.
43. Inoue, Y., J. Inoue, G. Lambert, S. H. Yim, and F. J. Gonzalez. 2004. Disruption of hepatic C/EBPalpha results in impaired glucose tolerance and age-dependent hepatosteatosis. *J. Biol. Chem.* **279:** 44740–44748.
44. Yang, J., C. M. Croniger, J. Lekstrom-Himes, P. Zhang, M. Fenyus, D. G. Tenen, G. J. Darlington, and R. W. Hanson. 2005. Metabolic response of mice to a postnatal ablation of CCAAT/enhancer-binding protein alpha. *J. Biol. Chem.* **280:** 38689–38699.
45. Olofsson, L. E., M. Orho-Melander, L. William-Olsson, K. Sjoholm, L. Sjostrom, L. Groop, B. Carlsson, L. M. Carlsson, and B. Olsson. 2008. CCAAT/enhancer binding protein alpha (C/EBPalpha) in adipose tissue regulates genes in lipid and glucose metabolism and a genetic variation in C/EBPalpha is associated with serum levels of triglycerides. *J. Clin. Endocrinol. Metab.* **93:** 4880–4886.